JOURNAL OF CATALYSIS **158,** 102–108 (1996)
ARTICLE NO. 0011

Platinum/Ceria CO Oxidation Catalysts Derived from Pt/Ce Crystalline Alloy Precursors

Christopher Hardacre,[1] Trevor Rayment, and Richard M. Lambert[2]

Chemistry Department, Cambridge University, Cambridge CB2 1EW, England

Received March 9, 1995; revised August 15, 1995

Pt/Ce alloys treated with O_2, N_2O, or CO/H_2 yield Pt/ceria catalysts that are active for CO oxidation. The most active catalysts are produced by N_2O treatment of Pt_3Ce_7 at 720 K, which leads to the highest dispersion of both the Pt and ceria phases. This reflects the smaller exotherm, which occurs with N_2O, apparently a critical requirement for production of a highly active catalyst. The performance of these Pt_3Ce_7-derived catalysts is comparable with that of the best, recently announced, materials prepared by wet chemical techniques. In all cases, most of the active material is invisible to X-ray diffraction and the catalysts exhibit very low CO-titratable Pt area ($<$0.05 CO/Pt). Prereduction in H_2 at 570 K greatly enhances the reactivity of a given catalyst. CO TPR shows that highest activity correlates with a reduction state at ~510 K, suggesting metal-promoted CO oxidation by the ceria. It seems possible that this high activity is associated with ceria spillover onto Pt, the spillover being facilitated by atomic-level mixing of Pt and Ce in the alloy precursor.

INTRODUCTION

Highly active catalysts may be produced from crystalline rare-earth/transition-metal alloys by appropriate treatment of the precursor alloy with reactive gases. This results in phase separation to yield ultradispersed transition-metal particles in intimate contact with a rare-earth oxide (or hydride) phase. It seems likely that charge transfer between the solid phases and the production of a high density of lattice defects in the oxide component can endow these materials with exceptional catalytic properties. Examples of such catalysts produced from alloy precursors include those for methanol synthesis (1–4), ammonia synthesis (5–8), alkene hydrogenation (9–13), and methane production (14–21). By way of illustration, we note that Cu/Nd_2O_3 catalysts produced in this way are very active for methanol synthesis at temperatures as low as 350 K, at which point the best available industrial catalysts are totally inactive (1, 4). In the majority of cases, the onset of high activity is found to coincide with the emergence of small transition-metal particles detectable by X-ray diffraction (XRD). In the case of methanol and ammonia synthesis catalysts produced from alloy precursors, it was concluded that the transition-metal was the active phase. However, Nix *et al.* (1) showed that there was little correlation between observed particle size and catalytic activity. Much of the active phase was XRD invisible, implying the presence of particles with diameters less than ~25 Å; the activity was therefore ascribed to both visible and ''invisible'' transition-metal particles.

Here we report the CO oxidation activity of a series of Pt/ceria catalysts derived from Pt_2Ce and Pt_3Ce_7 alloys using a variety of activation procedures. It is found that the material produced by oxidation of Pt_3Ce_7 with N_2O is very active and outperforms Pt/ceria catalysts prepared by wet impregnation.

EXPERIMENTAL

The alloy samples were prepared by rf induction heating: repeated melting and solidification ensured that the components were sufficiently mixed. Samples were crushed and sieved to yield a particle size between 50 and 250 μm and ~0.1 g of the alloy precursor was used in each experiment. Precursor activation and ultimate catalytic performance were examined over a range of conditions using *in situ* XRD in a single pass reactor with gas chromatographic detection. The experimental arrangement has been described in detail elsewhere (1). The XRD/reactor cell was mounted on a Siemens D500 diffractometer with a position sensitive detector for measurements with Cu$K\alpha$ radiation. Correlated observations of solid phases and the associated chemical behaviour can provide a powerful means of identifying catalytically significant effects. Analysis of the XRD data was performed by fitting Cauchy, pseudo-Voigt, or Split Pearson functions to the peaks. From these fits an estimate of the amount of X-ray visible material was obtained by reference to standards prepared

[1] Present address: Chemistry Department, Queen's University, Belfast, BT9 5AJ, Northern Ireland.

[2] To whom correspondence should be addressed.

0021-9517/96 $12.00

from Pt and CeO_2. The Scherrer equation was used to obtain an average particle size; in general, the peak shapes indicated a wide distribution of particle size in the final active catalysts.

Catalyst testing was achieved by ramping the temperature of the catalyst in a 1%/0.5% CO/O_2 mix (balance N_2); conversion of CO to CO_2 was monitored in the gas chromatograph. For purposes of comparison, the temperature for 50% conversion (T 50%; light off) was taken as a measure of the absolute activity: a decrease in T (50%) indicating an increase in activity. This conversion corresponds to a CO_2 production rate of $\sim(3.4 \times 10^{-7}$ mol/(s-gram of catalyst). In all cases a catalyst charge of ~0.1 g was used with a total flow rate of ~10 cm^3/min. The typical space velocity was 5000/h. Following activation, the alloy-derived catalysts were tested as made, i.e., *raw*, and also after reduction in 1 bar H_2 at 570 K for 1 h, i.e., *prereduced.*

TPR catalyst characterisation was performed in flowing 10% H_2/Ar mix (~5 cm^3/min), whilst ramping the temperature from 300 to 1100 K at ~12 K/min. Hydrogen consumption was measured with a katharometer by comparing the thermal conductivities of the gas from the reactor with that of a reference stream. The exit gas was passed through a cryogenic trap ahead of the katharometer to remove water formed by this reduction process. Due to the high sensitivity of the apparatus, small sample charges were used, typically ~10 mg. To reduce weighing errors the samples were diluted using silica powder. The latter is stable below 1070 K and our technique is based on the procedure of Robertson *et al.* (22).

Temperature-programmed CO reduction (TPCOR) traces were obtained on passing a 2.5%CO/He mix at ~30 cm^3/min over the samples, whilst ramping the temperature from 300 to 820 K at 10 K/min. Exit gases were analysed using a VG Q7 quadrupole mass spectrometer. By monitoring CO^+ (28 amu) and CO_2^+ (44 amu), the formation of CO_2 due to CO reduction of the sample could be followed. The apparatus has been fully described elsewhere (23), and it was also used for CO surface area measurements by adsorption frontal chromatography. Research grade gases were used throughout the work. Temperatures and Pt particle sizes were measured to an accuracy of ±5°C and ±20%, respectively.

RESULTS

Activation of the Alloy Precursors

Two different Pt–Ce alloys were studied (Pt_2Ce and Pt_3Ce_7) and these produced catalysts with significantly different structural and reactive properties. In every case except that of treatment in pure H_2, activation led to the formation of CeO_2. In the case of Pt_3Ce_7, XRD-visible Pt was also produced. *In situ* XRD data acquired during precursor activation in various gas atmospheres are shown in Figs. 1–4. In the case of the Pt_2Ce samples, all the XRD patterns exhibit small peaks present at $2\theta \sim 43°$ due to the cell. All features in the XRD patterns of the Pt_2Ce and Pt_3Ce_7 precursors correspond well with previously reported crystal structures for these alloys (24, 25).

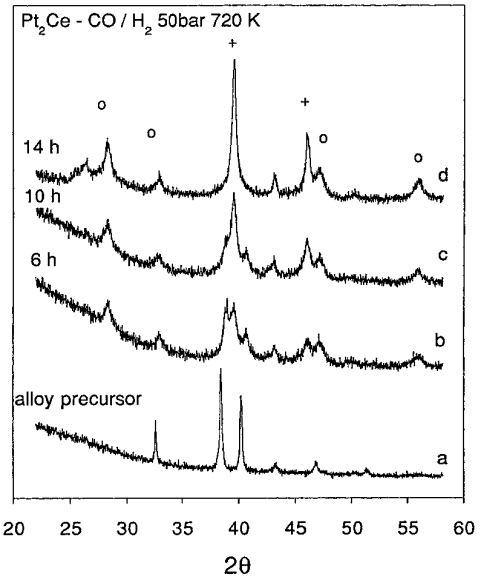

FIG. 1. *In situ* XRD traces following the activation of Pt_2Ce in 50 bar CO/H_2 at 720 K: (a) as received, (b) 6 h activation, (c) 10 h activation, and (d) 14 h activation. (○) CeO_2 and (+) Pt peaks.

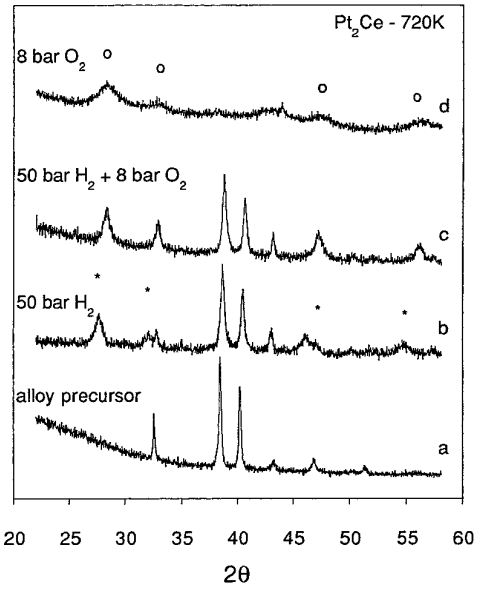

FIG. 2. Comparison of *in situ* XRD traces following the activation of Pt_2Ce in (a) as received, (b) 50 bar H_2 at 720 K, (c) 50 bar H_2 at 720 K plus 8 bar O_2 at 720 K, and (d) 8 bar O_2 at 720 K. (*) CeH_{2+x}, (○) CeO_2 peaks.

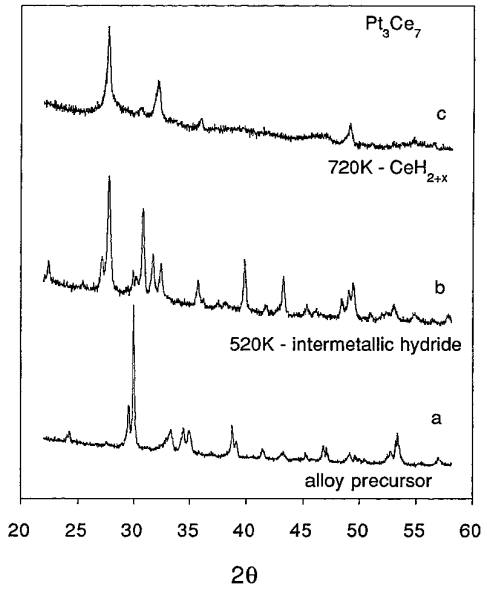

FIG. 3. *In situ* XRD traces following the activation of Pt_3Ce_7 in 50 bar H_2 at (a) 300 K, showing the alloy phase, (b) 520 K, showing the intermetallic hydride, and (c) 720 K, showing the formation of CeH_{2+x}.

Activation in 1/2 CO/H_2 was studied because earlier work showed (1, 4) that this treatment leads to the production of extremely active methanol synthesis catalysts from Cu/rare-earth alloys. For the same reason, we investigated the effects of prehydrogenating the alloy because subsequent oxidation of the resulting intermetallic hydrides can provide a low-temperature route to very small metal particles (1). Activation of both alloys in CO/H_2 at 50 bar led to formation of XRD-visible Pt particles and CeO_2, with complete disappearance of the alloy diffraction features by 720 K. Pt particle size data are summarised in Table 1 for Pt_2Ce and in Table 2 for Pt_3Ce_7. The Pt_2Ce alloy was much the less reactive of the two: even at 720 K, complete transformation of the alloy occurring required 14 h of activation, compared to 1 h for Pt_3Ce_7. In the former case, the small invariant feature at $2\theta \sim 27°$ does not correspond to any diffraction features due to the alloy, CeO_x or Pt. It is due to a change in background intensity and is an artefact associated with a change in catalyst texture (and possibly a shift in sample position).

The two alloys differed in their reactivity towards hydrogen. In the case of Pt_2Ce, reaction with H_2 at 50 bar and 720 K led to formation of the nonstoichiometric hydride CeH_{2-x}, although complete transformation of the alloy phase was not possible, even after prolonged treatment at this temperature. CeH_{2-x} was also produced upon activation of Pt_3Ce_7 under the same conditions. However, in this case it was formed via an intermediate phase, thought to be an intermetallic Pt/Ce hydride. The intermetallic hydride is characterised by a 6% expansion in the alloy lattice and the complete absence of any other phase. In both cases, subsequent oxidation of CeH_{2-x} in N_2O or O_2 at 370–430

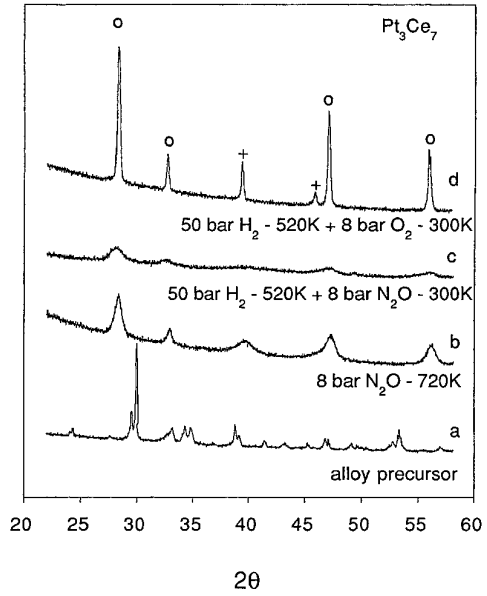

FIG. 4. Comparison of *in situ* XRD traces following the activation of Pt_3Ce_7 in (a) as received, (b) 8 bar N_2O at 720 K, (c) 50 bar H_2 at 520 K plus 8 bar N_2O at 300 K, and (d) 50 bar H_2 at 520 K plus 8 bar O_2 at 300 K. (+) CeH_{2+x}, and (○) CeO_2 peaks.

TABLE 1

CO Oxidation Activity of Pt_2Ce-Derived Catalysts and "Wet Route" Catalysts

Activation procedure	T (50%)(K)		Pt particle size(Å)
	Raw	Prereduced	
None	400	395	—
Hydrogen at 720 K, 50 bar	410	—	52
N_2O/O_2 at 720 K, 8 bar	450	395	—
CO/H_2 at 720 K, 50 bar	<5% at 570 K	<5% at 570 K	125
Hydride + N_2O/O_2 at 520 K, 8 bar	450	400	—
Hydride + CO/H_2 at 520 K, 8 bar	450	450	—
0.9% wt Pt/75% wt Al_2O_3–25% wt CeO_2 catalyst prepared by wet impregnation	490	390	—
0.9% wt Pt/CeO_2 catalyst prepared co-precipitation	400	335	—

Note. Pt particle sizes calculated using the Scherrer equation.

TABLE 2

CO Oxidation Activity of Pt_3Ce_7-Derived Catalysts

Activation procedure	*T* (50%)(K)		Pt particle size(Å)
	Raw	Prereduced	
None	490	490	—
Hydrogen at 520 K, 50 bar	390	390	—
Hydrogen at 720 K, 50 bar	460	440	—
N_2O at 720 K, 8 bar	395	355	35
O_2 at 720 K, 8 bar	450	400	35
CO/H_2 at 720 K, 50 bar	450	415	29
Intermetallic + N_2O at 520 K, 8 bar	480	425	11
Intermetallic + O_2 at 520 K, 8 bar	<5% at 520 K	<5% at 520 K	160
Intermetallic + CO/H_2 at 520 K, 8 bar	520	520	30
Hydride + N_2O at 520 K, 8 bar	490	490	11
Hydride + O_2 at 520 K, 8 bar	490	490	23
Hydride + CO/H_2 at 520 K, 8 bar	520	520	30

Note. Pt particle sizes calculated using the Scherrer equation.

K was rapid, forming CeO_2 and, in the case of Pt_3Ce_7, XRD-visible Pt.

Oxidative reaction of the intermetallic hydride was much more dramatic: O_2 at 300 K led to complete transformation of the whole sample to Pt and CeO_2 with quantitative conversion of all the starting alloy. Reaction was accompanied by a substantial exotherm, yielding large particles of both ceria and Pt. In this case an apparent 40°C temperature rise was observed; the actual temperature rise of the catalyst is not known but is likely to have been significantly higher due to the heat capacity of the thermocouple and cell components in thermal contact with the sample. The occurrence of such a large temperature excursion is strongly suggested by the observed sintering of the catalyst, as detected by XRD. This is to be contrasted with the results of all the other procedures which generated catalysts consisting mainly of XRD-invisible material, indicating either particle sizes <25 Å or a high degree of disorder. With N_2O and CO/H_2 activation, the intermetallic hydride did not give a detectable exotherm and the resulting catalysts consisted of much smaller particles.

Direct oxidation of both Pt_2Ce and Pt_3Ce_7 alloys in 8 bar of N_2O or O_2 led to CeO_2 formation at 470 K with complete transformation occurring at 720 K. Only in the case of the Pt_3Ce_7 alloy was XRD-visible Pt detected after activation, and there was little difference between the XRD patterns resulting from O_2 and N_2O activation. However, with both alloy precursors, much of the Pt- and Ce-containing material in the activated catalyst remained XRD invisible even after complete transformation of the starting alloy.

Catalyst Testing

Each alloy-derived catalyst was tested for activity towards CO oxidation. In addition, for purposes of comparison, two Pt/ceria catalysts prepared by wet chemical methods were tested under exactly the same conditions. Catalyst A was prepared by impregnation using chloroplatinic acid to give a loading of 0.9% wt Pt on 75% wt Al_2O_3–25% CeO_2. Catalyst B was a very active material prepared by coprecipitation using chloroplatinic acid and Ce $(NO_3)_3 \cdot 6H_2O$ exactly according to a recently published patent (26), again resulting in a loading of 0.9% wt Pt on CeO_2. Both catalysts were dried at 380 K and then calcined at 570 K. *T* (50%) light-off temperature data are presented in Table 1 for Pt_2Ce-derived catalysts, along with comparison data for catalysts A and B. Table 2 shows corresponding data for Pt_3Ce_7-derived catalysts. Interestingly, precursors activated solely in an oxidising gas always resulted in the highest activity. Prehydrogenation had a detrimental effect, and, in contrast with methanol synthesis catalysts prepared from Cu/rare-earth alloys (1, 4), CO/H_2 treatment produced less active catalysts compared with N_2O and O_2 activation. It is also striking that the Pt-rich alloy

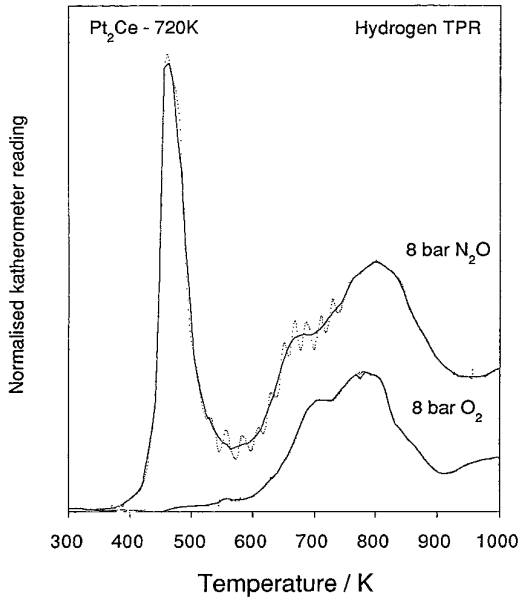

FIG. 5. H_2 TPR traces following activation of Pt_2Ce at 720 K in 8 bar of N_2O and O_2.

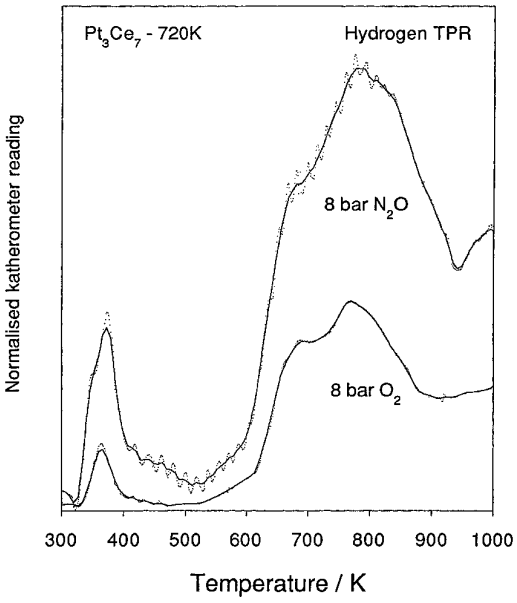

FIG. 6. H_2 TPR traces following activation of Pt_3Ce_7 at 720 K in 8 bar of N_2O and O_2.

(Pt_2Ce) systematically produced less active catalysts than Pt_3Ce_7. In every case, reduction at 570 K in 1 bar H_2 for 1 h *after* activation increased catalytic activity, but produced no change in the XRD. Inspection of the activity data makes it is clear that XRD does not show the whole picture: for example, there are few structural differences between the Pt_3Ce_7-derived catalysts following activation in N_2O and O_2, yet the *activity* is very different in the two cases.

TPR Characteristics

TPR profiles were recorded using both CO and H_2 as reducing agents following activation of both alloys in specific environments. Figures 5 and 6 show the results obtained following activation in N_2O and O_2. Both alloys show significant reduction states above 670 K during H_2 TPR. There are also states at 370 and 470 K following N_2O or O_2 activation of Pt_3Ce_7 and after N_2O activation Pt_2Ce, respectively. For each alloy, the relative efficacy of the activation procedures may be estimated by normalising the reduction peak areas to sample weight. This procedure reveals a trend in which N_2O activation increases the number of reducible sites in comparison with O_2 activation. The corresponding TPCOR results are shown in Fig. 7. Little reduction was found for catalysts derived from both alloys following activation in O_2, whereas in both cases substantial reduction was observed after activation in N_2O. The most noteworthy features are the reduction peaks between 500 and 620 K. For comparison, CO TPR profiles for the catalysts prepared by impregnation and coprecipitation are also shown in Fig. 7.

CO Surface Area Measurements

The CO-titratable surface area of all the alloy-derived catalysts was <0.05 CO/Pt both before and after reduction in H_2 at 570 K.

DISCUSSION

As with methanol (1–4) and ammonia (5–8) catalysts, activation of rare-earth alloys provides a route for the synthesis of highly active CO oxidation catalysts. However, in the present case, activation in CO/H_2 and prehydrogenation are not useful strategies. In both these cases it is possible that the water produced during oxidation of the hydride or intermetallic hydride to CeO_2 results in poisoning of the oxide, possibly by formation of a stable surface hydroxide. Such poisoning could inhibit oxygen storage by the ceria component, which is thought to play an important role in oxidation catalysis (27, 28).

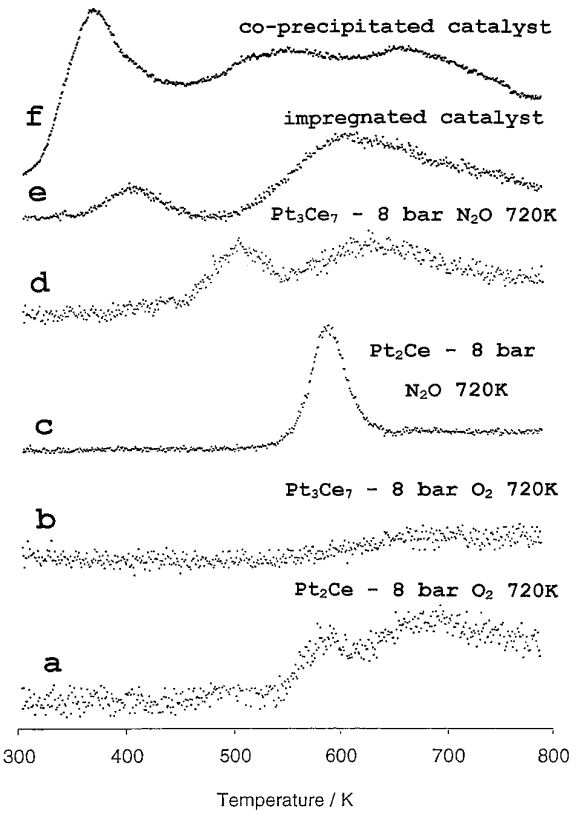

FIG. 7. CO TPR traces following activation of (a) Pt_2Ce and (b) Pt_3Ce_7 at 720 K in 8 bar of O_2, (c) Pt_2Ce and (d) Pt_3Ce_7 at 720 K in 8 bar of N_2O, (e) the 0.9% wt Pt/75% wt Al_2O_3–25% wt CeO_2 catalyst prepared by wet impregnation, and (f) the 0.9% wt Pt/CeO_2 catalyst prepared coprecipitation.

The most interesting behaviour was observed after activation in either N_2O or O_2 alone. XRD indicates that the structure of the various activated catalysts is similar, yet their CO oxidation activities differ significantly. We therefore conclude that the activity for CO oxidation is due to XRD-invisible material: indeed Pt_2Ce-derived catalysts are active even though no Pt is detected by XRD. However, the TPR results are revealing in this respect.

The hydrogen TPR data provide some indication as to the dispersion of the Pt and ceria phases. This is important because in many of the cases described above, much of the material in the final catalyst was invisible to XRD due to either small particle size or disorder: in such circumstances the observed X-ray line broadening is not a useful guide to dispersion.

Hydrogen TPR states above 670 K are due to reduction of ceria: Yu Yao *et al.* (27, 29) have assigned the state at ~750 K to reaction with "capping" oxygen, whereas states above 820 K are due to the formation of Ce_2O_3. Reduction states above 920 K are attributed to bulk reduction of ceria. The intensity of states below 920 K gives an indication of the ceria particle size—smaller particles giving rise to increased intensity. In the case of N_2O activation of both alloys, the greater intensity of reduction features at temperatures below 920 K, relative to O_2 activation, indicates that N_2O activation always generates smaller oxide particles.

The reduction states below 490 K are interesting and in good accord with the information provided by XRD. All these states may be assigned to reduction of platinum oxide (30). It has been shown that the exact reduction temperature depends on the degree of crystallinity of the Pt oxide—the lower the temperature the more crystalline the oxide. With Pt_2Ce, no XRD-visible Pt was detected on activation in either O_2 or N_2O. The corresponding TPR data show a peak at ~470 K, indicating the presence of amorphous Pt oxide. However, with Pt_3Ce_7, the activated catalyst *did* contain XRD-visible Pt and this was accompanied by a TPR peak at 370 K—indicating the presence of crystalline Pt oxide. We may therefore infer that amorphous Pt oxide forms poorly crystalline or very highly dispersed, XRD-invisible Pt upon reduction, whereas crystalline Pt oxide yields larger, crystalline, XRD-detectable Pt particles. It then follows that there is XRD-invisible Pt in the catalyst produced by N_2O activation of Pt_3Ce_7 alloy-derived catalyst, as denoted by the ~470 K shoulder present in the TPR data.

N_2O activation of both alloys led to increased intensity of the Pt oxide reduction states as compared with O_2 activation: N_2O produces smaller metal particles. This improved dispersion of both the ceria and Pt phases in the final catalyst results in the highest activity, found in the Pt_3Ce_7-derived catalysts. Comparison with published hydrogen TPR data for Pt/CeO_2 catalysts (31) shows that in the present case peaks indicative of metal–support interaction are absent. This indicates that either no such interaction exists, or, more likely, that the corresponding reduction state is below 300 K. Such TPR states below 300 K are indeed observed for the very active Pt/CeO_2 catalyst produced by coprecipitation (32), and they are not observed with the conventionally prepared catalyst. The TPCOR data show the presence of a state that correlates with high activity for CO oxidation. The most active catalyst (N_2O-activated Pt_3Ce_7) exhibits a reduction state at 510 K which is not assignable to the reduction of either oxide: Pt oxide reduces at 370–470 K and CeO_2 above 670 K. Given that the CO oxidation activity of the N_2O-activated Pt_3Ce_7-derived catalyst is significantly superior to that of ostensibly similar catalysts made by conventional wet impregnation methods and comparable with that of the catalyst prepared by coprecipitation, it seems likely that the ~510 K TPCOR feature is due to a metal–support interaction; a similar feature appears upon reduction of the coprecipitated catalyst, but not on reduction of the less active catalyst prepared by impregnation. Thus the ease of reducibility by CO is consistent with CO oxidation taking place via a redox mechanism in which the enthalpy for O vacancy creation in the ceria is lowered by the metal–support interaction as discused below (33, 34).

Why does N_2O-activated Pt_3Ce_7 alloy produce the most active catalyst? There appear to be two closely related reasons. First, N_2O reacts with both alloys far less vigorously than O_2 which should result in a smaller exotherm, hence yielding smaller particles. Different temperature excursions were not detectable for activation in N_2O or O_2 alone, due to the finite heat capacity of the system in contact with the sample. However, such differences *were* readily detected on oxidising the intermetallic hydride formed from the Pt_3Ce_7 alloy; a 40° exotherm in the case of O_2 activation *versus* no temperature rise with N_2O. Second, Pt_3Ce_7 is more readily oxidised than Pt_2Ce (reaction at 570 and 720 K, respectively). Both effects work in the same direction—Pt_3Ce_7 undergoes oxidation by N_2O at a relatively low temperature and with a small exotherm: sintering is minimised and the Pt–CeO_2 interaction increased.

Traditionally, CO-titratable metal surface area has been used as a measure of metal dispersion, high dispersions being associated with high activity. In the present case, and with the coprecipitated Pt–CeO_2 catalysts (31), the CO-titratable surface area is small. Nevertheless, the activity for CO *oxidation* is very high. This implies either low dispersion (unlikely) or spillover of the support (ceria) onto the metal (Pt). The second explanation seems more plausible and gains support from recent spectroscopic and kinetic studies (35) carried out with model $Pt(111)/CeO_2$ catalysts. These indicated that the fully CeO_2-encapsulated single crystal (with no CO titratable Pt area) was a much better CO oxidation catalyst than clean Pt (111), and we discussed a model for promotion of the oxide by the metal

(32). According to the model proposed in Ref. (32), Pt promotes oxygen vacancy formation in the ceria overlayer, thus greatly increasing the oxide's activity towards CO oxidation via abstraction of lattice oxygen. In the present case, full encapsulation of the metal by the oxide may not occur: instead, an SMSI effect due to decoration of the Pt by ceria may be responsible for the enhanced activity, by analogy with the reported behaviour of Pt/titania catalysts (e.g., 36, 37). It seems plausible that atomic-level mixing of the Pt and Ce components in the alloy precursor should facilitate such effects, provided that the phase separation does not occur too vigorously.

CONCLUSIONS

1. N_2O activation of Pt/Ce alloys produces the best catalysts. A highly active CO oxidation catalyst may be produced by N_2O activation of Pt_3Ce_7: this material exhibits activity comparable with the best commercial Pt/CeO_2 catalysts.

2. The activity of these alloy-derived catalysts does not correlate with the XRD data, indicating that catalysis is largely due to XRD-invisible material.

3. TPCOR features at ~510 K are ascribed to Pt-promoted reduction of CeO_2; this state is only present in high activity catalysts.

4. Much smaller Pt and CeO_2 particles were obtained on activation in N_2O than O_2. This reflects the smaller exotherm which occurs with N_2O, apparently critical for production of a highly active catalyst.

5. It seems likely that the high activity is associated with ceria-encapsulated Pt, the encapsulation being facilitated by atomic-level mixing of Pt and Ce in the alloy precursor.

ACKNOWLEDGMENTS

We acknowledge financial support by the EPSRC under Grant GR/J00632. C.H. holds an EPSRC Research Fellowship and is a Research Fellow of Emmanuel College, Cambridge. C.H. acknowledges the award of an EPSRC CASE studentship sponsored by Johnson Matthey plc. We are indebted to Helen Hatcher of Johnson Matthey plc for supplying catalysts A and B.

REFERENCES

1. Nix, R. M., Rayment, T., Lambert, R. M., Jennings, J. R., and Owen, G., *J. Catal.* **106,** 216 (1987).
2. Shaw, E. A., Rayment, T., Walker, A. P., and Lambert, R. M., *Appl. Catal.* **67,** 151 (1990).
3. Shaw, E. A., Rayment, T., Walker, A. P., Jennings, J. R., and Lambert, R. M., *J. Catal.* **126,** 219 (1990).
4. Jennings, J. R., Lambert, R. M., Nix, R. M., Owen, G., and Parker, D. G., *Appl. Catal.* **50,** 157 (1989).
5. Panov, G. I., and Kharitonov, A. S., *React. Kinetic Catal. Lett.* **29,** 267 (1985).
6. Walker, A. P., Ph.D. thesis, Cambridge, 1989.
7. Walker, A. P., Rayment, T., and Lambert, R. M., *J. Catal.* **117,** 102 (1989).
8. Walker, A. P., Rayment, T., Lambert, R. M., and Oldman, R. J., *J. Catal.* **125,** 67 (1990).
9. Vann Vucht, J. H. N., Kuijpers, F. A., and Bruning, H. C. A. M., *Philips Res. Repts.* **25,** 133 (1970).
10. Soga, K., Imamura, H., and Ikeda, S., *J. Phys. Chem.* **81,** 1762 (1977).
11. Soga, K., Imamura, H., and Ikeda, S., *Chem. Lett.,* 1387 (1976).
12. Soga, K., Imamura, H., and Ikeda, S., *J. Catal.* **56,** 119 (1979).
13. Imamoto, T., Mita, T., and Yokoyama, M., *J. Chem. Soc. Chem. Commun.,* 163 (1983).
14. Wallace, W. E., Elatter, A., Takeshita, T., Coon, V. T., Bechman, C. A., and Craig, R. S., *in* "Proceedings, 2nd International Conference on Electr. Str. Activ., Wroclaw Poland V-8," 1976.
15. Coon, V. T., Takeshita, T., Wallace, W. E., and Craig, R. S., *J. Phys. Chem.* **80,** 1878 (1976).
16. Imamura, H., and Wallace, W. E., *J. Catal.* **65,** 127 (1980).
17. Shamsi, A., and Wallace, W. E., *Ind. Eng. Chem. Prod. Res. Dev.* **22,** 582 (1983).
18. Moldovan, A. G., Elatter, A., and Wallace, W. E., *J. Solid State Chem.* **25,** 23 (1978).
19. Chin, R. L., Elatter, A., Wallace, W. E., and Hercules, D. M., *J. Phys. Chem.* **84,** 2895 (1980).
20. Luengo, C. A., Cabrera, A. L., MacKay, H. B., and Maple, M. B., *J. Catal.* **47,** 1 (1977).
21. Barrault, J., Guilleminot, A., Achard, J. C., Paul-Boncour, V., Percheron-Guegan, A., Hilaire, L., and Coulon, M., *Appl. Catal.* **22,** 273 (1986).
22. Robertson, S. D., McNicol, B. D., de Baas, J. M., Kloet, J. M., and Jenkins, J. W., *J. Catal.* **37,** 424 (1975).
23. Nix, R. W., Judd, R. W., Lambert, R. M., Jennings, J. R., and Owen, G., *J. Catal.* **118,** 175 (1989).
24. Dwight, A. E., *Trans. Am Soc. Met.* **53,** 479 (1961).
25. Olcese, G. L., *J. Less Common Metals* **33,** 71 (1973).
26. Rajaram, R. R., Ansell, G. P., and Hatcher, H. A., European Patent Application, EP 0602 865 A1 (1993).
27. Yao, H. C., and Yu Yao, Y.-F., *J. Catal.* **86,** 254 (1984).
28. Harrison, B., Diwell, A. F., and Hallet, C., *Platinum Met. Rev.* **32,** 73 (1988).
29. Yu Yao, Y.-F., *J. Catal.* **87,** 152 (1984).
30. McCabe, R. W., Wong, C., and Woo, H. S., *J. Catal.* **114,** 354 (1988).
31. Shyu, J. Z., and Otto, K., *J. Catal.* **115,** 16 (1989).
32. Rajaram, R. R., Ansell, G. P., and Hatcher, H. A., European Patent Application, EP 0602 865 A1 (1993).
33. Frost, J. C., *Nature* **334,** 577 (1988).
34. Hardacre, C., Ormerod, R. M., and Lambert, R. M., *J. Phys. Chem.* **98,** 10901 (1994).
35. Hardacre, C., Ormerod, R. M., and Lambert R. M., *J. Phys. Chem.* **98,** 10901 (1994).
36. Belzunegui, J. P., Rojo, J. M., and Sanz, J., *J. Phys. Chem.* **95,** 3463 (1991).
37. Sadeghi, H. R., and Henrich, V. E., *J. Catal.* **82,** 279 (1984).